Effects of vertical magnetic field on impact dynamics of ferrofluid droplet onto a rigid substrate

Jiandong Zhou and Dengwei Jing*
State Key Laboratory of Multiphase Flow in Power Engineering and International Research Center for Renewable Energy, Xi'an Jiaotong University, Xi'an 710049, China

(Received 31 January 2019; published 26 August 2019)

Ferrofluid as a smart fluid has a wide range of applications. Although the spreading dynamics of water droplets have been well investigated, spreading dynamics of ferrofluid droplets under a magnetic field has rarely been studied. This paper reports our findings of the impact dynamics of a ferrofluid droplet onto a tempered glass surface in the presence of a vertical magnetic field. The effects of magnetic intensity, impact velocity, and Fe_3O_4 nanoparticle concentration were investigated. It turned out that with the increased magnetic intensity, the height of the ferrofluid droplet would decrease owing to the energy dissipation increase of ferrofluids under a magnetic field and the additional stretching force in the vertical direction. Interestingly, we found that exertion of the magnetic field could significantly diminish the influence of velocity differences on the droplet spread dynamics in height direction. Satellite droplets were also observed in certain cases when the rebound kinetic energy could overcome the restraint of surface tension and adhesion of viscosity in the presence of the magnetic field. Our work will be a significant reference to with regard to various practical applications, especially when the impact dynamics of ferrofluid droplets need to be under precise control, for instance, as in three-dimensional printing or spray coating, etc.

DOI: 10.1103/PhysRevFluids.4.083602

I. INTRODUCTION

Droplet impact exists in many industrial processes, besides being a common phenomenon in nature, such as raindrops [1], and the propagation of many forms of life, include fungi and bacteria [2–4]. Impact also plays an important role in spray coating [5], fuel injection [6], surface cooling [7], and ink-jet printing [8]. Generally, after impact of a droplet, it will undergo the process of spreading, recoiling, or splashing, and the dynamics of spreading and splashing are a critical issue for using droplet impingement in those industrial applications. There is much early experimental and numerical research investigating the behavior of droplet impacts on a surface; however, most of these works focus on pure liquid droplets or pure liquid addition to a surfactant. Denis *et al.* investigated the contact time of a bouncing water drop after impacting a solid surface [9]. The results showed that contact time does not depend on the impact velocity under the range of velocities 20–230 cm/s. Wang *et al.* [10] studied pure water droplet dynamic behavior in the process of impact and spreading. Two different substrates were chosen for testing. They found that water droplets on glass oscillate only a few cycles before reaching an equilibrium shape, while it takes more than 28 cycles on a paraffin substrate. This means that the dynamics of impact and spreading also depend on the material properties of the substrate. Alizadeh *et al.* investigated the impact dynamics of water droplets on surfaces changing from being hydrophilic to superhydrophobic in the temperature range of −15 °C to 85 °C [11]. It was concluded that the droplet spread diameter can be significantly

*Corrsponding author: dwjing@mail.xjtu.edu.cn

affected by the substrate temperature when the substrate is hydrophilic. However, a weaker effect was observed on the hydrophobic substrate. Besides water droplets, some research has also focused on ethylene glycol and glycerin droplets [12–14]. In addition, surfactant is often added in pure liquid to study its impingement behavior. Chiang *et al.* [15] investigated the impact dynamics of sodium dodecyl sulfonate (SDS) surfactant solution impinging on polycarbonate surfaces. The effects of surface tension, impact velocity, and surface roughness were studied. The results showed that the effect of surface roughness on the drop dynamics for SDS solution is more obvious than that for pure water. Moreover, the oscillation of drop height of SDS solution is much weaker than that of pure water. Surfactant-enhanced spreading studies have been well reviewed in literature [16]. As a good example, it was found that after addition of surfactant, droplets become close to pancake shaped, and the macroscopic contact angle could be below 8° [17]. There often exists an optimal surfactant concentration for achieving a maximum spreading rate. Fast spreading of surfactant solutions over hydrophobic substrates has been explained by many mechanisms, including caterpillar motion at a three-phase contact line [18], direct transfer of surfactant molecules [19], formation of bilayers [20,21], Marangoni flow [22], etc.

On the other hand, magnetic nanofluids are suspensions comprised of a nonmagnetic base fluid and magnetic nanoparticles. The suspensions can be called smart or functional fluids, because fluid flow, particle movement, and the heat transfer process can be controlled by applying magnetic fields [23]. The possibility to induce and control the heat transfer process and fluid flow by means of an external magnetic field opened a window to a spectrum of promising applications, including magnetically controlled thermophysical properties for technological purposes, enhancement of heat transfer for cooling of high-power electric transformers, and magnetically controlled heat transfer in energy conversion systems [24–27].

Due to their magnetic field response, ferrofluids have been attempted in a drug tagged for cancer treatment [28]. It was also useful for restricting undesirable vibrations and to reduce the size of heat exchangers [29]. Ferrofluids are also used in digital electronics as a logic gate by coupling magnetic and hydrodynamic forces on the droplets [30]. Most recently, ferrofluids have found potential applications in three-dimensional (3D) printing due to their simplicity and adaptability to numerous complex shape requirements [31,32]. In 3D printing of metal, the shape distortion of a metal object is dictated by the droplet spreading dynamics during the laser-induced curing, and hence droplet spreading dynamics is one of the key parameters of lateral resolution in 3D printing [33,34]. Considering the above important applications, it is therefore urgent to investigate the spreading dynamics after ferrofluid droplet impact on the substrate. In fact, we have found that even with nonmagnetic nanoparticles, drop vibrations after impact can be obviously changed [35]. However, to the best of our knowledge, although many researchers have considered magnetowetting [36–38], manipulation of ferrofluid droplet movement [36,39,40], and the dynamics of droplet spreading while impinging on a substrate, these dynamics have not been studied under the influence of a magnetic field. It is necessary to enrich knowledge in this field to provide an essential reference for their applications.

In the present study, the spreading dynamics of a droplet after impacting a rigid surface under a vertical magnetic field are experimentally investigated. The magnetic field intensity, droplet impact velocity, and ferromagnetic particle concentration are all considered. First, for the droplet spreading diameter, recoiling height evolutions were quantified with accuracy and analyzed. Then the effects of impact velocity and magnetic intensity on spreading dynamics under vertical magnetic fields were studied. Finally, we observed satellite droplet formation and tried to find the underlying mechanism for this interesting phenomenon.

II. EXPERIMENTAL APPROACH

A. Materials

The ferrofluids used in this work were obtained by a two-step method. The nanoparticle concentrations are 0.01 and 0.1 wt %, respectively. Magnetite Fe_3O_4 nanoparticles with a diameter

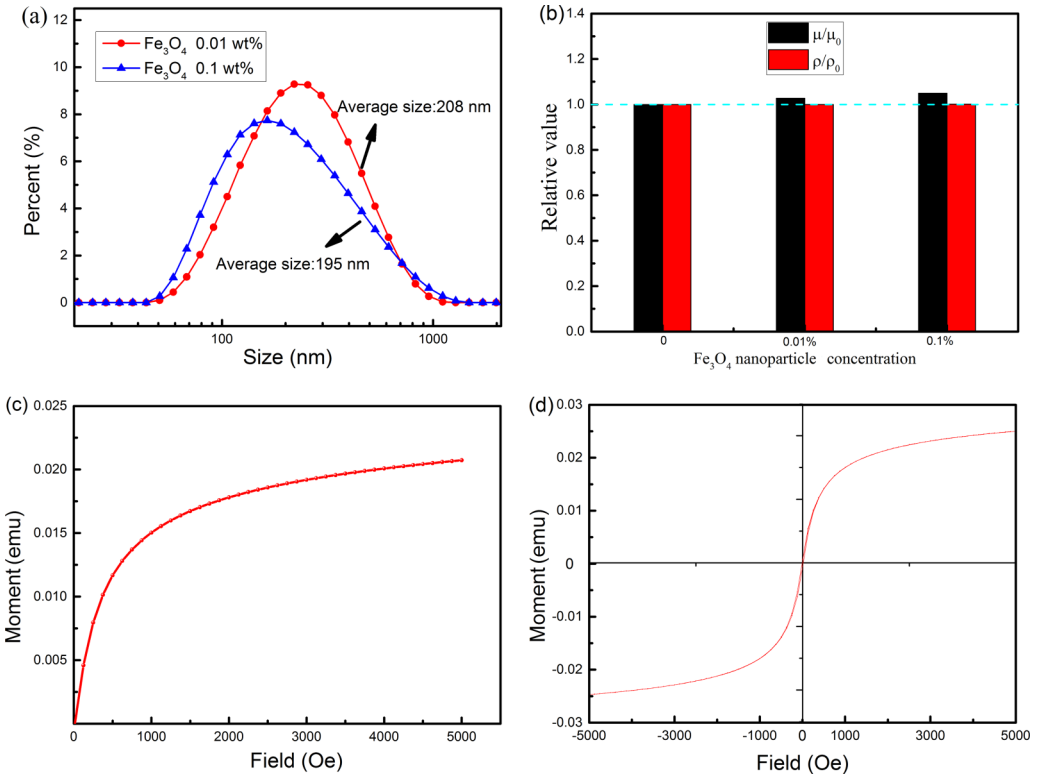

FIG. 1. (a) Particle size distribution in ferrofluids of three different mass fractions, (b) comparison of density and viscosity between ferrofluids with different nanoparticle concentrations, (c) magnetization curve of Fe_3O_4 nanoparticles, and (d) hysteresis loop of Fe_3O_4 nanoparticles.

of around 20 nm were from Aladdin (China). In order to guarantee a stable enough dispersion, a surfactant of sodium oleate (SO) and polyethylene glycol 4000 (PEG-4000) were used to allow the particles to disperse stably. For the preparation of ferrofluid, first, Fe_3O_4 nanoparticles were suspended in deionized water and subjected to ultrasonication for 30 min at a frequency and amplitude of 25 kHz and 60%, respectively. Then the first surfactant SO with weight ratio of surfactant to nanoparticle of 1:1 was added to the water followed by another 10 min of sonication. Finally, a second surfactant PEG-4000 was added, with mass fraction and sonication time the same as the second step. After these three steps, a stable water-based colloidal suspension of Fe_3O_4 nanoparticles coated with SO as the primary layer and PEG-4000 as the secondary layer can be obtained [41,42]. In order to confirm the homogeneity of dispersion, the ζ potential and particle diameter distribution were measured by using a Zetasizer Nano-ZS90. Generally, a suspension with a ζ potential of 30–40 mV, 40–60 mV, and above 60 mV (absolute value) correspond to general stability, better stability, and excellent stability, respectively [43,44]. The measured results showed that the ζ potential of suspension used in this study is 62.9 and 57.5 mV (absolute values), indicating that the nanoparticles are dispersed stably. Further, we also measured the nanoparticle diameter distribution with the dynamic light scattering (DLS) method.

Figure 1(a) shows that most of the nanoparticles in the suspension have sizes around 200 nm. The specific data indicated that average particle sizes are 208 and 195 nm, respectively, for the cases of nanoparticle concentrations of 0.01% and 0.1%. Apparently, due to the addition of surfactant, the nanoparticle suspension could still be well dispersed, although a certain extent of aggregation has occurred. Considering that many possible effects could be happening due to the addition of particles,

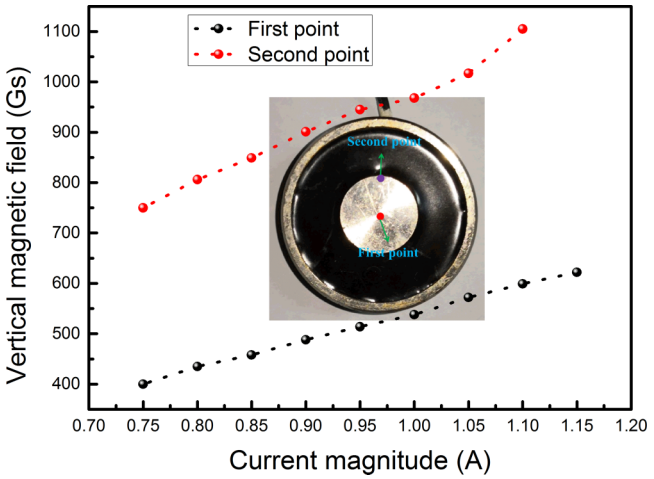

FIG. 2. Magnetic intensity as a function of the current magnitude.

even if the magnetic field was not applied, as a control experiment we measured the viscosity, contact angle, and density of the studied ferrofluid, respectively, with various nanoparticle mass fractions in the absence of a magnetic field to find out the possible effects of the nanoparticle itself on the physicochemical properties of the fluid. The results are shown in Fig. 1(b). It can be clearly seen that the addition of nanoparticles has a negligible effect on the density and viscosity of fluid in the absence of magnetic field. For the equilibrium contact angle, it changed from 89.3° to 60.3° when the nanoparticle concentrations were changed from 0.01% to 0.1%. It should also be noted that in our experiments, we have investigated each case with a constant nanoparticle concentration, which means that the change of contact angle due to nanoparticle addition has no influence on our studied processes. Figures 1(c) and 1(d) show the magnetization curve and hysteresis loop of the Fe_3O_4 nanoparticles employed in this study. One can see that they exhibit apparent superparamagnetism.

To ensure that the droplet has an appropriate contact angle and that droplet spreading can be clearly observed, the substrate should have an appropriate surface energy. Accordingly, a tempered glass surface was used as a substrate in our study. The surface was rectangular in shape with thickness of 0.4 mm and $145 \times 70\,\text{mm}^2$ size. After each set of experiments, the substrate was cleaned repeatedly by ethyl alcohol and water. Considering that substrate surface roughness also influences the dynamics of the droplet after impinging [45], the substrate surface roughness determined by the absolute roughness R_a has been specified. Here, measured with a TR200 roughness meter, the R_a value was determined to be 0.014 μm.

The magnetic field plays a key role in this work. Initially, we chose the NdFeB grade-N35 permanent magnet but found that its magnetic field intensity could not meet the experimental needs or be controlled accurately. Therefore, in order to achieve a controllable and appropriate magnetic field, an electromagnet was used in this study. The magnetic field intensity could be changed by adjusting the current magnitude. The relation between vertical magnetic field and current magnitude is presented in Fig. 2. It is evident that the magnetic field intensity in vertical direction is increased with the current magnitude, showing a nearly linear relationship. As shown by the inset in Fig. 2, two points on the electromagnet surface were chosen for obtaining a large range of magnetic field intensity, 0–1000 G.

B. Experimental setup

As presented in Fig. 3, the whole experimental system consisted of three subsystems: a droplet generation system, recording system, and a backlight system. A droplet generation system was used

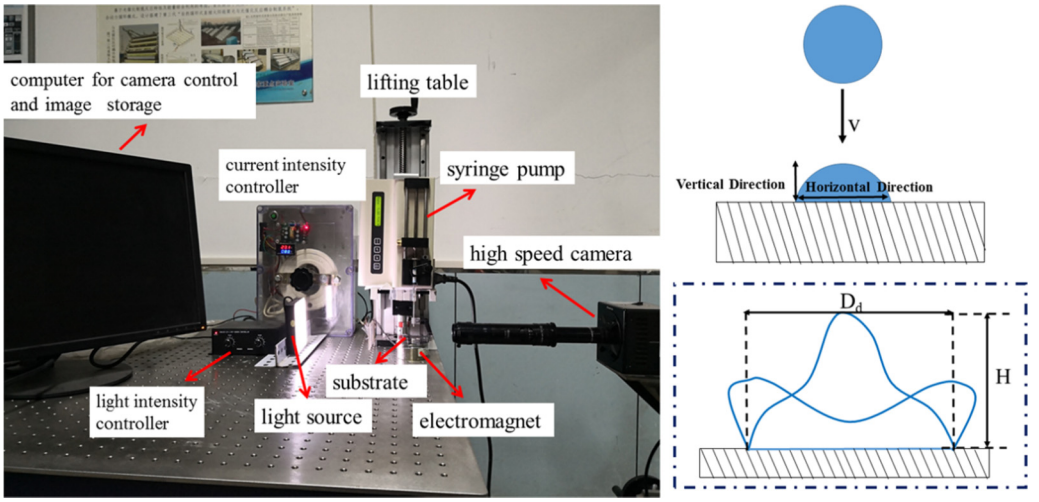

FIG. 3. Schematic diagram of experimental system.

to generate drops, including a syringe pump, an injector, and a raising platform. The syringe pump is on the raising platform; it can change the droplet impact velocity by adjusting the platform height. A single drop is formed from a fine needle, which then detaches from the needle tip due to its own weight under gravity. The recording system includes a desktop computer and a high-speed camera (Photron Fastcam Mini UX50). It is worth noting here that a camera with high enough speed is essential for the rapid and continuous recording of images of the drop as it impacts and spreads. There is also related software for recording, storing, and analyzing drop shape data. The framing rate of the high-speed camera is 1000 images per second in this work. The backlight system is composed of a light-emitting diode (LED) area light source and a current controller. This LED area light source can provide brightness uniformity to ensure a clear picture. The entire apparatus is placed on a precisely designed vibration isolation table to avoid the possible influence of external vibration.

III. RESULTS AND DISCUSSION

Generally, after impacting a substrate, a droplet will experience the process of spread, recoil, and oscillation, and this oscillation process will repeat periodically, accompanied by quick damping as recorded in Fig. 4. As shown from Fig. 4(a) to Fig. 4(c), at first, the droplet impact starts with a point contact with the surface and then spreads with a sharp increase in diameter until reaching its maximum diameter at the same time with the minimum thickness. Then, due to the stored interfacial energy, the droplet attempts to minimize the surface area so that the drop recoils and rebounds to its maximum height [Figs. 4(c)–4(e)]. However, the drop does not retract back to its initial status, which is assumed to be due to the prewetted surface [Fig. 4(f)]. After several times of periodical oscillations, it finally terminates. In order to acquire the data of oscillation quantitatively, the digital image processing technology was employed to analyze all the images from the experiments under various conditions. To be comparable, the moment when the droplet reaches its maximum radius [Fig. 4(c)] is chosen as the starting time in all the cases discussed below.

In order to investigate the effect of magnetic field on the droplet spreading dynamics, a vertical magnetic field was added and the magnetic intensity was adjusted to be 0, 400, 700, and 1000 G, concretely. The impact velocity was $U = 0.86\,\mathrm{m/s}$, and the Fe_3O_4 nanoparticle concentration was 0.1 wt %. Figure 5 shows the history of droplet shape change after impacting a surface. Here, in order to make appropriate comparisons, the diameter and height of the drop are transformed to the

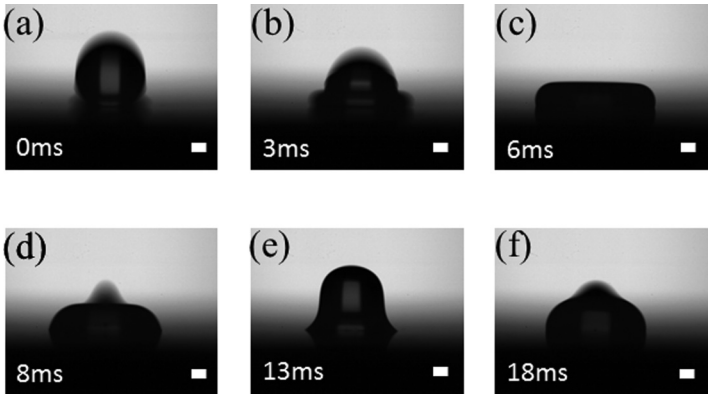

FIG. 4. The shape changes of droplets after impacting a substrate surface. The length of the scale bars corresponds to 0.6 mm, and the nanoparticle concentration is 0.01 wt % in the absence of magnetic field.

dimensionless forms D_d/D_0 and H_d/D_0. From the pictures it can be seen that oscillation occurs in both horizontal and vertical directions, and the droplet spreading behavior is not monotonic. Comparing the oscillation characteristics in two directions orthogonal with each other [Figs. 5(a) and 5(b)], it can be found that damping of oscillation in the horizontal direction is much easier and the vibration is more obvious in the vertical direction.

Specifically, in the horizontal direction, as shown in Fig. 5(a), the oscillation is strong within the initial 20 ms, and after that the oscillation becomes quickly damped. It was also found that addition of a magnetic field exerted little effect on the droplet spreading and oscillation in the horizontal direction. There is almost no difference between the situations of adding and not adding a magnetic field for the dimensionless diameter, vibration amplitude, and vibration frequency parameters. It should be noted here that whether or not there is an external magnitude, the continuous damping of the vibration could always be observed. Such damped oscillations could thus, at least in part, be attributed to the existence of surface tension [46] and viscous dissipation [47].

In the vertical direction, the oscillation amplitude and frequency are all stronger than in the horizontal direction within the whole range measurement range of 55 ms. In addition, unlike the case for the dimensionless diameter D_d/D_0, the dimensionless height H_d/D_0 is decreased with

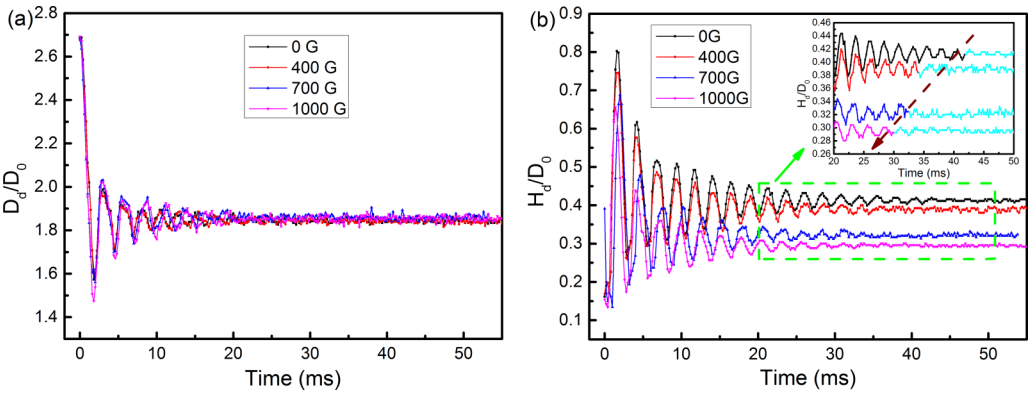

FIG. 5. Droplet spreading dynamics under vertical magnetic field at $U = 0.86\,\mathrm{m/s}$: (a) dimensionless diameter D_d/D_0, (b) dimensionless height H_d/D_0 as a function of time with 0.1% mass fraction Fe_3O_4 nanoparticles in varying magnetic fields.

the magnetic field strength, which can be clearly seen in Fig. 5(b). Moreover, H_d/D_0 shows a monotonic decrease with increased magnetic intensity. Except for what has been mentioned above, one can also note that the duration of vibration is decreased with the increment of magnetic field intensity. As shown by the inset in Fig. 5(b), as the intensity of the magnetic field increases, the vibration will decay faster, as indicated by the brown arrow in the inset, indicating that addition of a vertical magnetic field could suppress the vibration of ferrofluid droplets in the vertical direction. This phenomenon could be attributed to the increased magnetic intensity that would lead to incremental energy dissipation. On the one hand, in the impact process, except for the air resistance, the energy of a droplet could be dissipated in several ways after the first impact, including translational kinetic energy, oscillating kinetic energy, and energy dissipated by viscosity and surface tension, etc. The viscous losses can be quantified [11] using the following equation:

$$\mathrm{Viscous_{loss}} = \frac{\pi}{3}\rho \mathrm{V}^2 \mathrm{d}\mathrm{d}_{\mathrm{max}}^2 \frac{1}{\sqrt{\mathrm{Re}}}, \tag{1}$$

where d_{max} is the maximum spread diameter, V is the impact velocity, d is the initial droplet diameter, and Re is the Reynolds number corresponding to droplet impact conditions. The energy dissipated by the surface tension [48] is

$$\mathrm{Wst} = 2\mathrm{A}\gamma_{\mathrm{LG}}(\cos\theta_{\mathrm{R}} - \cos\theta_{\mathrm{A}}), \tag{2}$$

where A is the liquid-solid contact area, γ_{LG} is the surface tension between air and liquid, and θ_{R} and θ_{A} are receding and advancing angles.

On the other hand, it has also been found that surface tension and viscosity of ferrofluids are a strong function of magnetic field strength [49,50]. An expression describing the change of viscosity η_{r} as a function of the strength of the magnetic field H is in the form

$$\eta_{\mathrm{r}} = \frac{3}{2}\phi'\eta_0 \frac{\alpha - \tanh\alpha}{\alpha + \tanh\alpha}\langle \sin^2\beta \rangle, \tag{3}$$

where η_0 denotes the viscosity of the fluid in the absence of a magnetic field, Φ' the volume concentration of magnetic particles, β the angle between vorticity and field direction, and $\langle \cdots \rangle$ denotes the spatial average. The parameter α is the ratio of magnetic and thermal energy of the particles,

$$\alpha = \frac{\mu_0 \mathrm{mH}}{\mathrm{kT}}, \tag{4}$$

where μ_0 denotes the vacuum permeability, m the particle's magnetic moment, H the magnetic field intensity, k Boltzmann's constant, and T the absolute temperature.

The equation capable of describing the surface tension of a water-based magnetic fluid under the changing external magnetic field and temperature is as follows:

$$\gamma = \gamma_0\{2.5 \times 10^{-3}(\mu_0 \mathrm{mH/kT})^{4/5} + 1\}. \tag{5}$$

The parameters in this equation were defined earlier. As shown in Eqs. (3)–(5), both viscosity and surface tension of ferrofluid will increase with the increment of magnetic intensity H; therefore, the energy dissipated by viscosity and surface tension will both increase, which could then suppress the droplet retracting. Consequently, as shown in Fig. 5(b), H_d/D_0 will decrease and the vibration decays even faster when the magnetic strength increases from 0 to 1000 G.

For potential applications, it is significant to identify the maximum change in the shape of drops during the entire spreading process, starting from drop deposition. It is common practice in a droplet impact investigation to study the maximum diameter and height of drops [11,51,52]. Accordingly, finding the relationship between the intensity of the applied magnetic field and the change of maximum diameter and height of the drop after impact will be more valued. Figure 6 shows the variation of the dimensionless maximum spreading diameter D_{max}/D_0 at $t = 0$ ms and the dimensionless maximum recoiling height, H_{max}/D_0 at $t = 1.6$ ms, as a function of magnetic

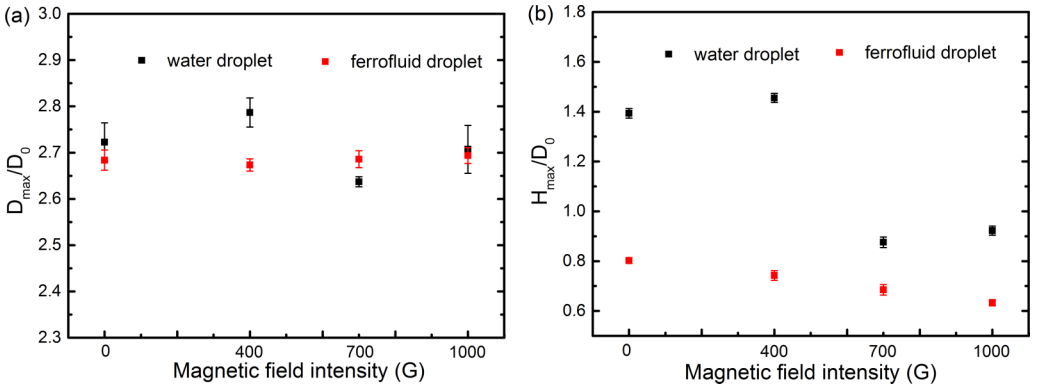

FIG. 6. (a) Dimensionless maximum spreading radius $D_{\max}/D_d$ at $t = 0$ ms and (b) maximum recoiling height $H_{\max}/D_d$ at $t = 1.6$ ms vs the magnetic field intensity for droplet without and with 0.1% nanoparticles, respectively.

field strength for a droplet without and with 0.1% nanoparticles, respectively. For a droplet without nanoparticles, as shown in Fig. 6(a), $D_{\max}/D_0$ obviously fluctuates with the increase of magnetic field intensity. A much more severe fluctuation for droplets without nanoparticles can be observed for the case of $H_{\max}/D_0$ as shown in Fig. 6(b). Since droplet impact is a violent turbulent process, instability is inevitable [53]. However, for the case of a 0.1 wt % ferrofluid droplet, the changing tendency of $D_{\max}/D_0$ and $H_{\max}/D_0$ is different—both the fluctuations are significantly inhibited compared to the case for a pure water droplet. The maximum dimensionless spreading diameter remains almost unchanged in the range of magnetic field investigated, as can be seen in Fig. 6(a). This confirms that the vertical magnetic field has little effect on ferrofluid droplet spread in the horizontal direction. In the vertical direction, it is obvious that the retraction height decreases with the increase of magnetic field intensity, as shown in Fig. 6(b), indicating that in the presence of a vertical magnetic field, the additional vertical stretching force significantly alters the height of the droplet. As shown in the literature [54], under a magnetic field parallel to the substrate surface, a water-based ferrofluid droplet surrounded by immiscible mineral oil would be stretched, so for the ferrofluid droplets under a magnetic field, there will be a magnetic pressure normal to the interface, which can be written as

$$p_n = \mu_0 H_n^2/2, \tag{6}$$

where n is the unit vector normal to the interface, and μ_0 and H are the permeability of vacuum and the applied field strength. Therefore, as presented in Eq. (6), with the increased magnetic field strength the magnetic pressure will be more obvious so that $H_{\max}/D_0$ will be decreased. This finding could be of value in accurate control of 3D printing.

In order to further investigate the magnetic effect on droplet spreading dynamics, the D_d/D_0 and H_d/D_0 at 53.4 ms of droplets with and without nanoparticles under various magnetic fields were selected for analysis. As shown by Fig. 7, first, it can be found that the D_d/D_0 of a water droplet is less than that of ferrofluid droplets, but for H_d/D_0, the situation is opposite. Second, for droplet with and without nanoparticles, the dimensionless diameter change trends are the opposite of the change trends of dimensionless height. Figure 7(a) shows that the D_d/D_0 of a ferrofluid droplet will increase very slightly when magnetic field intensity increases, but the D_d/D_0 of the water droplet remains nearly unchanged. Figure 7(b) shows that the H_d/D_0 for a water droplet is almost unchanged. However, H_d/D_0 of the ferrofluid droplet is significantly decreased with the incremental increase of magnetic field intensity. The phenomenon observed above could be explained with the help of the concept of paramagnetism [55]. The paramagnetism of the Fe_3O_4 nanoparticle used in this study has been confirmed by Figs. 1(b) and 1(c). Without the application of a magnetic field, the

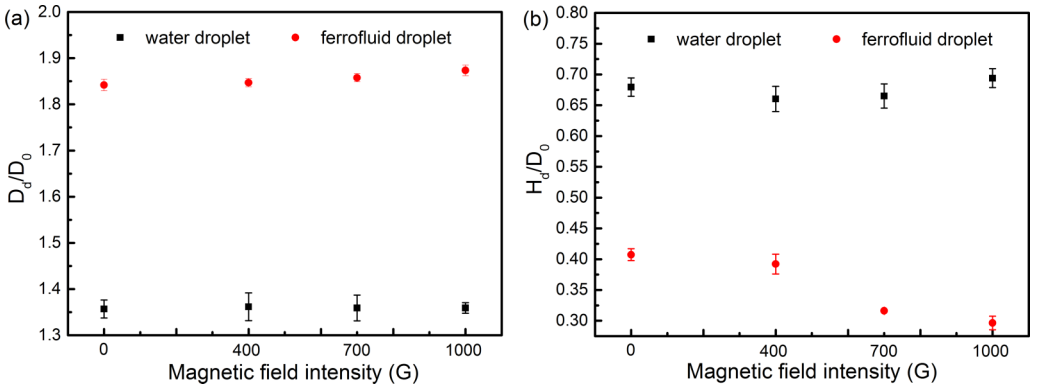

FIG. 7. Water and ferrofluid droplet spreading dynamics under vertical magnetic field at $U = 0.86$ m/s, $t = 53.4$ ms: (a) dimensionless diameter and (b) dimensionless height as a function of magnetic field intensity.

ferrofluid behaves as a liquid suspension. However, when an external magnetic field is applied, the atomic magnetic moments could reorient themselves along the field direction, resulting in a small net magnetization and positive susceptibility [51]. As the intensity of the applied field is increased, the net magnetization increases in line with the external field and the stretching force will increase, as discussed in Fig. 6. This could result in a bulk motion of fluid toward the magnetic field, which, in turn, results in the deformation of the interface or bulk of fluid drop. Of course, the above assumption is only preliminary based on our limited experimental data, and further experiments and theoretical analysis is needed in following studies.

Figure 8 shows the effects of magnetic field on the dynamics of droplet spreading with a magnetic field when impact velocity is different. Specifically, one impact velocity is 0.86 m/s and other one is 1.82 m/s, and the magnetic intensities are 0–1000 G, respectively. From the results, one can see that the $H_{\max}/D_0$ of droplet at 0.86 m/s is greater than that at 1.82 m/s. The same phenomenon has also been found in our previous work even in the absence of magnetic field [35]. According to traditional drop impact analysis, the spreading dynamics should be determined by the competition of several forces: impact initial kinetic energy, surface energy, and viscous dissipation, etc. It has

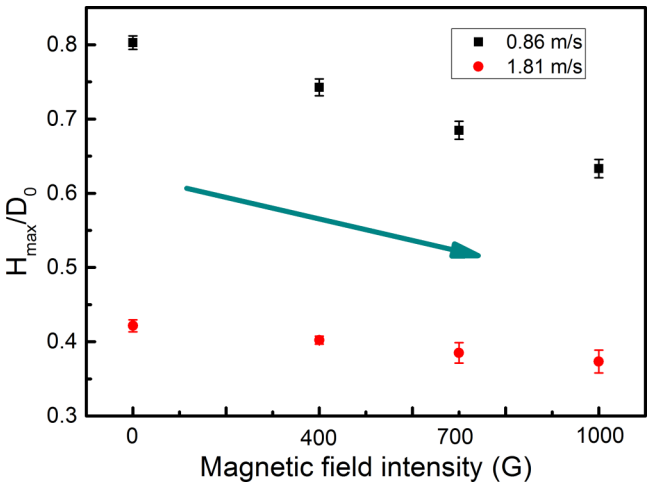

FIG. 8. Droplet spreading dynamics under vertical magnetic field: dimensionless height H_d/D_0 as a function of magnetic field with 0.1% mass fraction Fe_3O_4 nanoparticles and impact velocity $U = 0.86$ and 1.82 m/s when $t = 1.6$ ms.

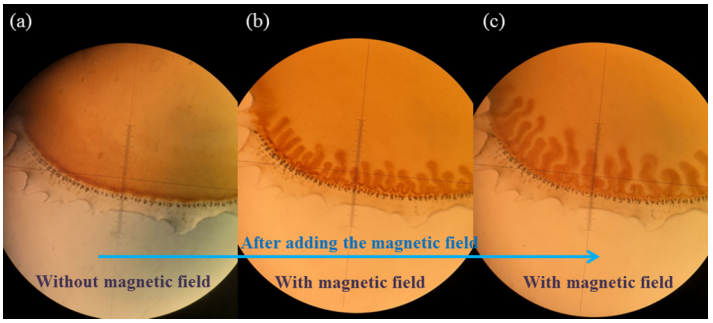

FIG. 9. Images showing particle movement in 0.1 wt % nanofluid droplets after applying the 1000-G magnetic field (a) in the absence of magnetic field, (b) 1 s after adding magnetic field, and (c) 2 s after adding magnetic field.

been proposed that with the impact velocity increase, the initial kinetic energy of the droplet is also increased, and therefore the thickness of the liquid film will become thinner for the large velocity [56,57]. Meanwhile, the initial kinetic energy will be consumed more in higher velocities and difficult to recoil. Therefore, in the high-impact velocity, $H_{\max}/D_0$ is small compared to that in low-impact velocities. It is important to note that the difference of H_d/D_0 between the cases of low velocity and high velocity versus magnetic field is less than that without a magnetic field, and the difference is reduced incrementally with magnetic intensity. In other words, addition of a magnetic field could diminish the influence of velocity differences on droplet spreading dynamics in the height direction. This finding could provide guidance if one wants to eliminate the impact velocity effects in various practical applications.

Why with the addition of magnetic field are there different values between two impact velocities in that the dimensionless height of the droplets are decreased? Besides the theoretical analysis regarding the incremental stretching force and energy dissipation of surface tension and viscosity, there is also an experimental phenomenon of increasing energy dissipation. On the one hand, the incremental increase of the magnetic field causes more internal molecular friction due to the rapid movement of suspended magnetite particles inside the fluid, which showed more resistance to damping initial kinetic energy and further against the droplet spreading [57]. Figure 9 vividly shows the movement of Fe_3O_4 nanoparticles after addition of a 1000-G magnetic field. It can be seen that the particles stay nearly static when there is no magnetic field. However, after adding the magnetic field, the particles start moving. On the other hand, with the incremental increase of magnetic strength, more powerful magnetic moments will be exerted on the particles, which could restrain the rotation of the magnetic particles in the fluid, causing increased friction between the particle and solvent layers; consequently, the viscosity of ferrofluids will increase [46]. As mentioned above, in the process of droplet spreading, energy dissipation plays an important role in the control of the dynamics and will depress spreading. Therefore, it is reasonable to deduce that movement of particles under a magnetic field is important in explaining the observed phenomena in our experiments.

Interestingly, the satellite droplets have also been observed in the experiment process, as shown in Fig. 10. However, this phenomenon only exists in the case of nanoparticle concentrations of 0.01 wt %, at $U = 0.8\,\mathrm{m/s}$ in the presence of a magnetic field. No such phenomenon of satellite droplets can be observed for the situations without a magnetic field or other Fe_3O_4 particle concentrations. As previously mentioned, the dynamics of droplet spreading, recoiling, and rebounding is dominated by initial kinetic energy, surface tension, and viscous dissipation. Therefore, one can speculate at this stage that with the application of magnetic field, retraction of kinetic energy could overcome the restraint of surface tension and adhesion of viscosity. This leads to the formation of one small satellite droplet separated from the main droplet in the opposite

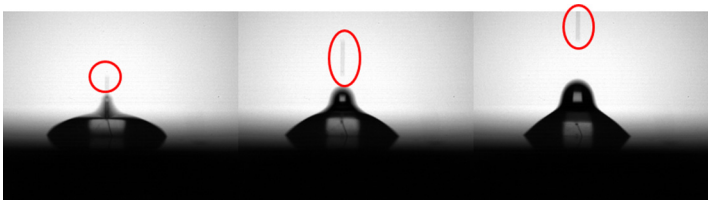

FIG. 10. Image of satellite droplet when magnetic intensities are 400, 800, and 1000 G, impact velocity is 0.8 m/s, and Fe_3O_4 nanoparticle concentration is 0.01 wt %.

direction of the impact velocity. Apparently, this finding could be of reference for some applications which contain the process of droplet impact, for example, satellite droplets have been found to be the main cause for contamination in 3D printing [33].

IV. CONCLUSION

In this work, we investigated the dynamic behavior of a ferrofluid droplet impacting a hydrophobic surface via the experimental method. Our aim is to explore how magnetic fields affect the collision characteristics of ferrofluids droplets, including its oscillation characteristic, maximum spreading diameter, maximum recoiling height, and effect of velocity difference on retraction height. Meanwhile, we also preliminarily analyzed the mechanism behind the experimental phenomena. The main conclusions of this work are summarized as follows:

(1) The addition of a vertical magnetic field has little effect on ferrofluid droplet spreading and oscillation in the horizontal direction. However, it plays an obvious role in the vertical direction. The dimensionless height H_d/D_0 shows a monotonic decrease with the increased magnetic intensity. In addition, with the increase of magnetic field intensity, the vibration will decay faster. Those phenomena are mainly attributed to the energy dissipation of viscosity and surface tension increasing incrementally with the magnetic intensity.

(2) In the horizontal direction, for droplets without Fe_3O_4 nanoparticles, D_{max}/D_0 will fluctuate in the range of magnetic field. For the ferrofluid droplet, however, the addition of a magnetic field could eliminate this fluctuation significantly. In the vertical direction, the H_{max}/D_0 of the water droplet also fluctuates, but as for the ferrofluid droplets, H_{max}/D_0 will decrease with the increased magnetic field intensity. Besides the energy dissipation increase, the stretching force is enhanced with increasing magnetic strength, which is assumed to be another reason for the H_{max}/D_0 decrease. In addition, the vertical magnetic field mainly acts in the vertical direction.

(3) The difference of H_d/D_0 between low velocity and high velocity with the magnetic field is less than that without the magnetic field, and the difference is reduced incrementally with the magnetic field intensity. It is also deduced that the incremental increase of ferrofluid viscosity and the vertical stretching force generated by the magnetic field are the main reasons for those observed phenomenon.

(4) Satellite droplets have also been observed in the experiments but only under certain conditions. Here, the rebound kinetic energy is assumed to be able to overcome the restraint of surface tension and adhesion of viscosity.

ACKNOWLEDGMENTS

The authors gratefully acknowledge financial support of the National Natural Science Foundation of China (No. 51776165) and Shanxi Science & Technology Co-ordination & Innovation Project (Contract No. 2017ZDXM-GY-067). This work was also supported by the China Fundamental Research Funds for the Central Universities and the financial support from Royal Society-Newton Advanced Fellowship grant (NAF\R1\191163).

[1] J. D. Mctaccart-Cowani and R. List, Collision and breakup of water drops at terminal, J. Atmos. Sci. **32**, 1401 (1975).
[2] T. Beneyton1, I. P. M. Wijaya, P. Postros, M. Najah, P. Leblond, A. Couvent, E. Mayot, A. D. Griffiths, and A. Drevelle, High-throughput screening of filamentous fungi using nanoliter-range droplet-based microfluidics, Sci. Rep. **6**, 27223 (2016).
[3] D. K. Kang, M. M. Ali, K. X. Zhang, S. S. Huang, E. Peterson, M. A. Digman, E. Gratton, and W. A. Zhao, Rapid detection of single bacteria in unprocessed blood using integrated comprehensive droplet digital detection, Nat. Commun. **5**, 5427 (2014).
[4] K. Wetzel, J. L. Cao, E. Kothe, and J. M. Köhler, Changing growth behavior of heavy-metal tolerant bacteria: Media optimization using droplet-based microfluidics, Eng. Life Sci. **15**, 327 (2015).
[5] Y. Zhang, D. Ge, and S. Yang, Spray-coating of superhydrophobic aluminum alloys with enhanced mechanical robustness, J. Colloid Interface Sci. **423**, 101 (2014).
[6] F. Drautz, K. Kumano, K. Machida, and H. Sauerland, *Development of Fuel Injection Control Technology in Gasoline Direct Injection Engine*, *Tagung Diesel-und Benzindirekteinspritzung 2014* (Springer Vieweg, Wiesbgaden, 2015), Vol. 9, p. 507.
[7] R. W. Maruda, G. M. Krolczyk, E. Feldshtein, F. Pusavec, M. Szydlowski, S. Legutko, and A. Sobczak-Kupiec, A study on droplets sizes, their distribution and heat exchange for minimum quantity cooling lubrication (MQCL), Int. J. Mach. Tools Manuf. **100**, 81 (2016).
[8] D. H. A. T. Gunasekera, S. L. Kuek, D. Hasanaj, Y. F. He, C. Tuck, A. K. Croft, and R. D. Wildman, Three-dimensional ink-jet printing of biomaterials using ionic liquids and co-solvents, Faraday Discuss. **190**, 509 (2016).
[9] R. Denis, C. Clanet, and D. Quéré, Surface phenomena: Contact time of a bouncing drop, Nature (London) **417**, 811 (2002).
[10] M. J. Wang, F. H. Lin, J. Y. Ong, and S. Y. Lin, Dynamic behaviors of droplet impact and spreading—Water on glass and paraffin, Colloids Surf., A **339**, 224 (2009).
[11] A. Alizadeh, V. Bahadur, S. Zhong, W. Shang, R. Li, J. Ruud, M. Yamada, L. H. Ge, A. Dhinojwala, and M. Sohal, Temperature dependent droplet impact dynamics on flat and textured surfaces, Appl. Phys. Lett. **100**, 111601 (2012).
[12] T. Lim, S. Han, J. Chung, J. T. Chung, S. Ko, and C. P. Grigoropoulos, Experimental study on spreading and evaporation of inkjet printed pico-liter droplet on a heated substrate, Int. J. Heat Mass Trans. **52**, 431 (2009).
[13] Š. Šikalo, C. Tropea, and E. N. Gani, Impact of droplets onto inclined surfaces, J. Colloid Interface Sci. **286**, 661 (2005).
[14] C. L. Tang, M. X. Qin, X. Y. Weng, X. H. Zhang, P. Zhang, J. L. Li, and Z. H. Huang, Dynamics of droplet impact on solid surface with different roughness, Int. J Multiphase Flow. **96**, 56 (2017).
[15] C. Y. Chiang, A. Casandra, W. Suryaputra, and S. Y. Lin, Drop impingement of water and aqueous SDS solution on polycarbonates, J. Ind. Eng. Chem. **49**, 189 (2017).
[16] N. M. Kovalchuk, A. Trybala, O. Arjmandi-Tasha, and V. Starov, Surfactant-enhanced spreading: Experimental achievements and possible mechanisms, Adv. Colloid. Interface Sci. **233**, 155 (2016).
[17] X. Wang, L.Q. Chen, E. Bonaccurso, and J. Venzmer, Dynamic wetting of hydrophobic polymers by aqueous surfactant and superspreader solutions, Langmuir **29**, 14855 (2013).
[18] V. Starov, Static contact angle hysteresis on smooth, homogeneous solid substrates, Colloid Polym. Sci. **291**, 261 (2013).
[19] K. P. Ananthapadmanabhan, E. D. Goddard, and P. Chandar, A study of the solution, interfacial and wetting properties of silicone surfactants, Colloids Surf. **44**, 281 (1990).
[20] E. Ruckenstein, Effect of short-range interactions on spreading, J. Colloid Interface Sci. **179**, 136 (1996).
[21] E. Ruckenstein, Superspreading: A possible mechanism, Colloid. Surfaces A **412**, 36 (2012).
[22] A. Chengara, A. Nikolov, and Darsh Wasan, Surface tension gradient driven spreading of trisiloxane surfactant solution on hydrophobic solid, Colloids Surf., A **206**, 31 (2002).
[23] A. Malvandi, S. A. Moshizi, and D. D. Ganji, Effect of magnetic fields on heat convection inside a concentric annulus filled withAl_2O_3-water nanofluid, Adv. Powder Technol. **25**, 1817 (2014).

[24] D. X. Song, D. W. Jing, J. F. Geng, and Y. X. Ren, A modified aggregation based model for the accurate prediction of particle distribution and viscosity in magnetic nanofluids, Powder Technol. **283**, 561 (2015).
[25] M. Hosseini, E. Mohammadianb, M. Shirvani, S. N. Mirzababaei, and F. Shakeri Aski, Thermal analysis of rotating system with porous plate using nanofluid, Powder Technol. **254**, 563 (2014).
[26] I. Nkurikiyimfura, Y. M. Wang, and Z. D. Pan, Heat transfer enhancement by magnetic nanofluids—A review, Renewable Sustainable Energy Rev. **21**, 548 (2013).
[27] D. X. Song, D. W. Jing, B. Luo, J. F. Geng, and Y. X. Ren, Modeling of anisotropic flow and thermodynamic properties of magnetic nanofluids induced by external magnetic field with varied imposing directions, J. Appl. Phys. **118**, 045101 (2015).
[28] A. Stephan Lübbe, C. Bergemann, H. Riess, F. Schriever, P. Reichardt, K. Possinger, M. Matthias, B. Dorken, F. Herrinann, R. Gurtler *et al.* Clinical experiences with magnetic drug targeting: A phase I study with 40-epidoxorubicin in 14 patients with advanced solid tumors, Cancer Res. **56**, 4686 (1996).
[29] S. W. Charles, Ferrofluids magnetically controllable fluids and their applications, Ferrofluids–Magn. Control. Fluids Appl. **594**, 3 (2002).
[30] G. Katsikis, J. S. Cybulski, and M. Prakash, Synchronous universal droplet logic and control, Nat. Phys. **11**, 588 (2015).
[31] B. Nagarajan, A. F. E. Aguilera, A. Qureshi, and P. Mertiny, in *ASME 2017 International Mechanical Engineering Congress and Exposition* (American Society of Mechanical Engineers, New York, 2017), p. V002T02A032.
[32] S. Manukyan and M. Schneider, Experimental investigation of wetting with magnetic fluids, Langmuir **32**, 5135 (2016).
[33] C. W. Visser, R. Pohl, C. Sun, G. W. Römer, B. Huis in 't Veld, and D. Lohse, Toward 3D printing of pure metals by laser-induced forward transfer, Adv. Mater. **27**, 4087 (2015).
[34] M. Zenou, A. Sa'ar, and Z. Kotler, Digital laser printing of aluminum micro-structure on thermally sensitive substrates, J. Phys. D: Appl. Phys. **48**, 205303 (2015).
[35] J. D. Zhou, Y. C. Wang, J. F. Geng, and D. W. Jing, Characteristic oscillation phenomenon after head-on collision of two nanofluid droplets, Phys. Fluids **30**, 072107 (2018).
[36] N. T. Nguyen, G. Zhu, Y. C. Chua, V. N. Phan, and S. H. Tan, Magnetowetting and sliding motion of a sessile ferrofluid droplet in the presence of a permanent magnet, Langmuir **26**, 12553 (2010).
[37] C. Rigoni, M. Pierno, G. Mistura, D. Talbot, R. Massart, J. C. Bacri, and A. Abou-Hassan, Static magnetowetting of ferrofluid drops, Langmuir **32**, 7639 (2016).
[38] S. Tenneti, S. G. Subramanian, M. Chakraborty, G. Soni, and S. DasGupta, Magnetowetting of ferrofluidic thin liquid films, Sci. Rep. **7**, 44738 (2017).
[39] A. Egatz-Gómez, S. Melle, A. A. García, S. A. Lindsay, M. Márquez, P. Dominguez-Garcia, M. A. Rubio, S. T. Picraux, J. L. Taraci, T. Ciement, D. Yang, M. A. Hayes, and D. Gust, Discrete magnetic microfluidics, Appl. Phys. Lett. **89**, 034106 (2006).
[40] N. T. Nguyen, K. M. Ng, and X. Huang, Manipulation of ferrofluid droplets using planar coils, Appl. Phys. Lett. **89**, 052509 (2006).
[41] R. Y. Hong, S. Z. Zhang, Y. P. Han, H. Z. Li, J. Ding, and Y. Zheng, Preparation, characterization and application of bilayer surfactant-stabilized ferrofluids, Powder Technol. **170**, 1 (2006).
[42] R. Hong, Z. Ren, Y. Han, H. Li, Y. Zheng, and J. Ding, Rheological properties of water basedFe_3O_4ferrofluids, Chem. Eng. Sci. **62**, 5912 (2007).
[43] J. H. Lee, K. S. Hwang, S. P. Jang, B. H. Lee, J. H. Kim, S. U. S. Choi, and C. J. Choi, Effective viscosities and thermal conductivities of aqueous nanofluids containing low volume concentrations ofAl_2O_3nanoparticles, Int. J. Heat Mass Transfer **51**, 2651 (2008).
[44] A. Ghadimi, R. Saidur, and H. S. C. Metselaar, A review of nanofluid stability properties and characterization in stationary conditions, Int. J. Heat Mass Transfer **54**, 4051 (2011).
[45] K. Range and F. Feuillebois, Influence of surface roughness on liquid drop impact, J. Colloid Interface Sci. **203**, 16 (1998).
[46] X. G. Zhang and O. A. Basaran, Dynamic surface tension effects in impact of a drop with a solid surface, J. Colloid Interface Sci. **187**, 166 (1997).

[47] S. C. Zhao, R. D. Jong, and D. V. D. Meer, Liquid-Grain Mixing Suppresses Droplet Spreading and Splashing during Impact, Phys. Rev. Lett. **118**, 054502 (2017).
[48] B. B. Wang, Y. P. Zhao, and T. X. Yu, Fabrication of novel superhydrophobic surfaces and droplet bouncing behavior, Part 2: Water droplet impact experiment on superhydrophobic surfaces constructed using ZnO nanoparticles, J. Adhesion Sci. Technol. **25**, 93 (2012).
[49] S. Odenbach, Recent progress in magnetic fluid research, J. Phys.: Condens. Matter **16**, R1135 (2004).
[50] S. Sudo, H. Hashimoto, and A. Ikeda, Measurements of the surface tension of a magnetic fluid and interfacial phenomena, JSME Int. J., Ser. 2, **32**, 47 (1989).
[51] D. Susan-Resiga and L. Vékás, Yield stress and flow behavior of concentrated ferrofluid-based magnetorheological fluids: The influence of composition, Rheol. Acta **53**, 645 (2014).
[52] A. Ahmeda, A. J. Qureshib, B. A. Fleck, and P. R. Waghmared, Effects of magnetic field on the spreading dynamics of an impinging ferrofluid droplet, J. Colloid Interface Sci. **532**, 309 (2018).
[53] M. Pack, P. Kaneelil, H. Kim, and Y. Sun, Contact Line Instability Caused by Air Rim Formation under Nonsplashing Droplets, Langmuir **34**, 4962 (2018).
[54] G. P. Zhu, N. T. Nguyen, R. V. Ramanujan, and X. Y. Huang, Nonlinear Deformation of a Ferrofluid Droplet in a Uniform Magnetic Field, Langmuir **27**, 14834 (2011).
[55] K. M. Krishnan, *Fundamentals and Applications of Magnetic Materials* (Oxford University Press, Oxford, UK, 2016).
[56] R. Patel, Effective viscosity of magnetic nanofluids through capillaries, Phys. Rev. E **85**, 026316 (2012).
[57] M. Pasandideh-Fard, Y. M. Qiao, S. Chandra, and J. Mostaghimi, Capillary effects during droplet impact on a solid surface, Phys. Fluids **8**, 650 (1996).